Chinese Chemical Letters 37 (2026) 111778

Contents lists available at ScienceDirect

Chinese Chemical Letters

journal homepage: www.elsevier.com/locate/cclet

Fluoride-induced sign inversion of circularly polarized luminescence of B,N-thia[8]helicene

Shuai Qiu[a,1], Jia Tang[a,1], Wan Xu[a], Zhiying Ma[a,*], Chao Zhang[a], Sheng Zhang[a,*], Chunli Li[a], Wei Tian[b,*], Hua Wang[a,*]

[a] Institute of Nanoscience and Engineering, Henan University, Kaifeng 475004, China
[b] Shaanxi Key Laboratory of Macromolecular Science and Technology, Xi'an Key Laboratory of Hybrid Luminescent Materials and Photonic Device, MOE Key Laboratory of Material Physics and Chemistry under Extraordinary Conditions, School of Chemistry and Chemical Engineering, Northwestern Polytechnical University, Xi'an 710072, China

ARTICLE INFO

Article history:
Received 7 May 2025
Revised 6 August 2025
Accepted 30 August 2025
Available online 31 August 2025

Keywords:
Helicene
Circularly polarized luminescence
Sign inversion
Fluoride ions

ABSTRACT

A novel thia[8]helicene (**BN[8]H**) with B,N heteroatoms incorporated in the molecular skeleton was synthesized *via* Suzuki coupling reaction and intramolecular direct electrophilic C–H borylation. Its helical structure was confirmed by X-ray crystal analysis. Enantiomers **BN[8]H** showed the interesting responses to fluoride ion stimulation with novel sign inversion of electronic circular dichroism (ECD) and circularly polarized luminescence (CPL). TD-DFT calculations revealed that the fluoride ions significant influence the transition dipole moments and $\theta_{u,m}$, resulting in circularly polarized luminescence reversal.

© 2026 Published by Elsevier B.V. on behalf of Chinese Chemical Society and Institute of Materia Medica, Chinese Academy of Medical Sciences.

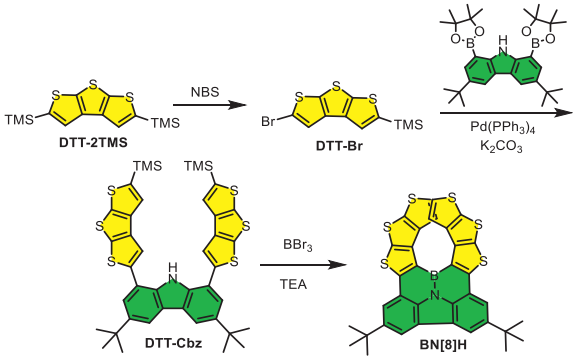
Organic molecules with circularly polarized luminescence (CPL) [1–3] have attracted significant research interest due to their potential applications in a variety of fields, including anti-counterfeiting, bioimaging and optical sensing [4–9]. External stimuli such as solvents, temperature, photons, and ions induced sign inversion of CPL in chiral systems can significantly increase the convenience of CPL materials [10–17]. Current strategies to control the sign inversion of CPL commonly focus on supramolecules systems, chiral small molecule species, liquid crystals and metal complexes [18–27]. However, at the molecular level, it is still a great challenge for switching the CPL sign to a given enantiomer without any chemical modification.

Recently, helicenes [28–33], defined as *ortho*-fused polycyclic aromatic compounds with helical molecular structures and inherent helical chirality, have considered as ideal candidates as CPL handedness switching materials due to their modifiability of the molecular skeleton and tunability of photo-physical and chiro-optical properties. For instance, combine helicenes with rigid twistacenes [34], motor-helicene hybrid system [35], oxidation or enhanced ICT modulation [36], combine helicene with responsive luminophore [37], change in the peripheral substituent of helicene [38], and heterohelicenes [39]. Among them, heteroaromatic helicenes showed impressive CPL response, especially the doping with neighboring boron–nitrogen (BN) units in helicene skeleton. Boron–nitrogen atoms, on the one hand, can endow helicenes with delocalized electronic structures, well-tunable excited-state photophysical properties, enhance their fluorescence quantum yield, and regulate half-maximum [40–46]. On the other hand, incorporating boron–nitrogen atoms into the appropriate positions in helicenes could also adjust the electric (μ) and magnetic (m) transition dipole moments to possibly change the $\theta_{u,m}$ and improve the luminescence dissymmetry factors (g_{lum}) values [47–49]. However, incorporating BN units into the skeleton of helicenes with CPL handedness switching still remains unexplored.

Herein, we report a facile and efficient synthesis of thia[8]helicene (**BN[8]H**) with BN unit and dithieno[2,3-*b*:3′,2′-*d*]thiophene (**DTT**) moiety [50]. Notably, **BN[8]H** exhibits moderate photoluminescence quantum yield and strong chiroptical properties. In addition, the novel sign inversion of both ECD and CPL were observed by adding certain amounts of tetra-*n*-butylammonium fluoride and boron trifluoride diethyl etherate. The theoretical calculation results show that the dipole moments and their angles of the magnetic and electric transitions of **BN[8]H** are changed by the addition of fluoride ions. This study establishes a new strategy to efficiently and conveniently adjust the handedness and intensity of CPL of helicenes, which may provide a universal platform for

* Corresponding authors.
E-mail addresses: mzy11@henu.edu.cn (Z. Ma), zhang.sheng.2022@henu.edu.cn (S. Zhang), happytw_3000@nwpu.edu.cn (W. Tian), hwang@henu.edu.cn (H. Wang).
[1] These authors contributed equally to this work.

https://doi.org/10.1016/j.cclet.2025.111778
1001-8417/© 2026 Published by Elsevier B.V. on behalf of Chinese Chemical Society and Institute of Materia Medica, Chinese Academy of Medical Sciences.



Scheme 1. Synthetic route to **BN[8]H**.

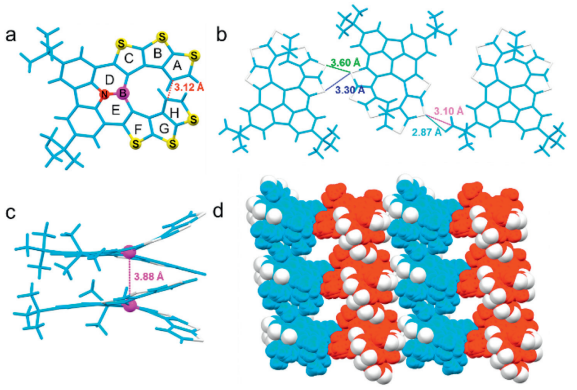


Fig. 1. (a) Molecular structures of **BN[8]H**. Solvent molecules were omitted for clarity for *rac*-**BN[8]H**. (b) showing S···S and S···H interactions, (c) a dimer of (*P*)-**BN[8]H** with one complementary B···B interaction (d) crystal packings.

future construction of helicenes based CPL-active smart materials and devices with promising application potentials.

The synthetic route to **BN[8]H** is shown in Scheme 1. The carbazole precursor **DTT-Cbz** was synthesized *via* a Suzuki coupling reaction with 3–bromo-dithieno[2,3-*b*:3′,2′-*d*]thiophene (**DTT-Br**) [51] and readily available borylated carbazole derivative in an excellent isolated yield up to 85 %. Introduction of boron atoms to the molecular structure by using boron tribromide as the boron source with triethylamine as the additive in *o*-dichlorobenzene (*o*-DCB) at 180 °C was achieved to produce **BN[8]H** in 78 % yield in gram scale. Standard spectroscopic techniques (proton nuclear magnetic resonance ^{1}H NMR, ^{13}C NMR, and high-resolution mass spectrometry-electrospray ionization mass spectrometry) of above compounds are shown in Supporting information.

The single crystal of *rac*-**BN[8]H** was obtained by slow evaporation in chloroform/methanol (3:1, v/v) solutions and characterized by single crystal X-ray diffraction analysis. *Rac*-**BN[8]H** belongs to monoclinic space group C_12/C_2. As shown in Fig. 1, the crystal structure of **BN[8]H** shows that two B,N-fused six-membered rings embedded in the center of helicene and displays a helical skeleton due to the steric hindrance from the terminal thiophene rings. The formation of B,N-hexagons results in smaller dihedral angle (40.96°, ring A and ring H) with shorter distance (3.12 Å, C14···C20) of thiophene rings, and the B–N bond lengths is 1.417 Å (Fig. S18 in Supporting information). In the crystal packing of *rac*-**BN[8]H**, two homochiral molecules form a dimer with an intermolecular distance of 3.88 Å (B···B) (Fig. 1c). There are multiple intermolecular interactions among the surrounding molecules from the neighboring unit cells. These included S1···S2: 3.30 Å, S2···S3: 3.60 Å, S6···H35B: 2.87 Å and S6···C35: 3.10 Å (Fig. 1b), resulting in the *rac*-**BN[8]H** crystal composed of *P* and *M* configurations with a ratio of 1:1, two kinds of dimers are in-volved and embedded to each other in the assembly columns, forming a two dimensional (2D) supramolecular sheet framework (Fig. 1d). The details of crystal structures and intra-molecular interactions in crystals are shown in Fig. S22 (Supporting information), and the crystal parameters are listed in Tables S7 (Supporting information).

The UV–vis absorption spectra of **BN[8]H** in CH_2Cl_2 exhibit lowest energy absorption bands corresponding to $S_0 \rightarrow S_1$ transitions at 410 and 392 nm, followed by two stronger bands at 330 nm and 268 nm, respectively. Time-dependent density functional theory (TD-DFT) calculations at the B3LYP/6–31G (solvent CH_2Cl_2) level of theory indicate that the lowest-energy absorption band is a superposition of two transitions (oscillator strengths *f* of 0.26 and 0.32) corresponding primarily to the HOMO to LUMO transition (Table S1 and Fig. S7 in Supporting information), where the HOMO is delocalized over the whole molecule, while the LUMO is predominantly confined to the carbazole moieties and BN-rings (Fig. S8 in Supporting information). The fluorescence maxima are positioned at 465, 461 and 467 nm in CH_2Cl_2, MeOH and MeCN, respectively (Fig. S9 in Supporting information). And the fluorescence quantum yield of **BN[8]H** is 1.89 % (Fig. S10a in Supporting information). Thus, **BN[8]H** basically shows a very weak solvatochromic effect.

Due to the empty orbital on the boron atom, **BN[8]H** is able to bond with Lewis bases and therefore changed its photoelectric properties. However, even by adding 6.0 equiv. tetrabutylammonium salts of Cl^-, Br^-, I^-, ClO_4^- and PF_6^- to a THF solution of **BN[8]H**, their solution UV–vis is and fluorescence spectra were basically unchanged (Fig. S11 in Supporting information). Interestingly, upon the addition of tetra-*n*-butylammonium fluoride (TBAF), an obvious absorption peak appeared at 424 nm and the fluorescence emission peak gradually shifted to 436 nm and the intensity increased significantly. The color of the solution changed from green to yellow, while the fluorescence quantum yield increased up to 12.31 % (Fig. S10b in Supporting information). The complexation constant and detection limit for TABF of **BN[8]H** calculated to be 1.05×10^4 L/mol and 26 nmol/L (Figs. S12 and 13 in Supporting information), respectively. The experimental results prove that **BN[8]H** has the potential application in the fields of sensors, smart materials and stimulus-responsive materials. When boron trifluoride diethyl etherate was added to the solution above, the UV–vis and fluorescence spectra reverted back (Fig. S14 in Supporting information), indicating that the coordination between fluorine and boron was reversible and can be cycled several times. The responsiveness of **BN[8]H** to fluoride ions is attributed to the high electronegativity, small atomic radius, and low energy state of fluoride ions, which enable them to match the energy level of boron's vacant orbital to form a stable complex with a tetrahedral geometry [52,53]. To gain further insight into the reason for the formation of B-F complexes, we performed DFT calculations on the B3LYP/6–31G(d,p) level. As shown in Table S3 (Supporting information), the Mayer bond order of B-F bond is 1.06, which is indicative of a strong interaction between boron and fluoride. However, the Mayer bond order of B-Cl bond only is 0.09, it is proved that chloride ions are difficult to form stable complexes with boron.

To further prove the coordination between fluorine and boron, the ^{1}H NMR titration experiments were performed before and after the addition of TABF in **BN[8]H**. As shown in Fig. 2c, when an excess of fluoride ion (6.0 equiv.) was added to ensure a complete reaction, the chemical shift of proton changed obviously, indicating that the 3-coordinated boron was converted to a 4-coordinated one.

We also got the single crystals of fluorinated complex with the tetracoordinated boron atom. As shown Fig. S19 (Supporting information), *rac*-**BN[8]H-F** belongs to monoclinic space group *P*-1. The titration of fluoride caused a significant change of the helical

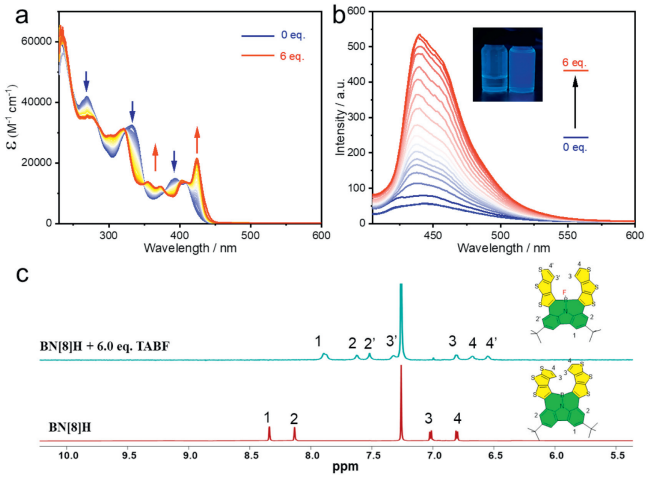


Fig. 2. Titration experiments of **BN[8]H** in THF solution with TBAF, measured by (a) UV–vis and (b) fluorescence spectra. Inset: photos showing fluorescence of **BN[8]H** and **BN[8]H-F**. (c) Partial ^{1}H NMR spectra of **BN[8]H**, with different equivalents of TABF ($CDCl_3$, 400 MHz, 298 K).

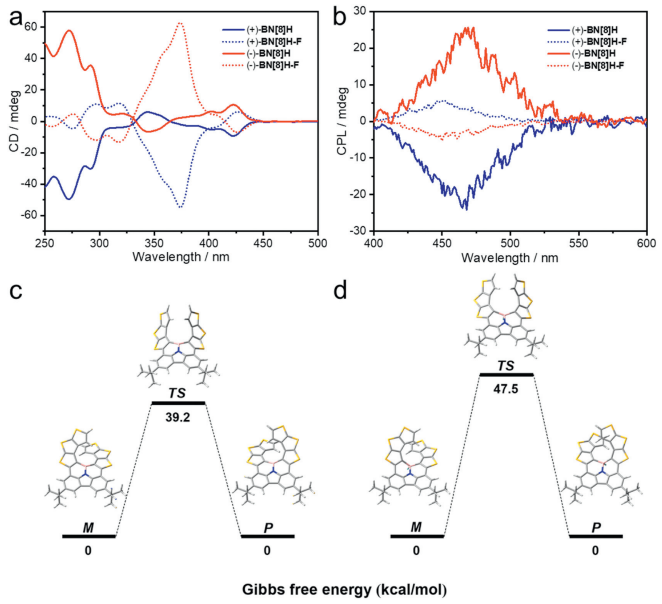


Fig. 3. Chiroptical properties. CD (a) and CPL (b) spectra of enantiomers **BN[8]H** in DCM. A pathway for the isomerization of (c) **BN[8]H** and (d) **BN[8]H-F** with relative Gibbs free energy as calculated at the B3LYP/6–31G(d,p) level.

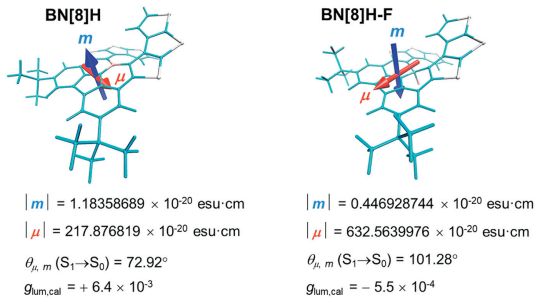


Fig. 4. Calculated electric transition dipole moment μ, magnetic transition dipole moment m, their angle $\theta_{u,m}$ and luminescence dis-symmetry factor ($g_{lum,cal}$) at $S_1 \rightarrow S_0$ of (a) **BN[8]H** and (b) **BN[8]H-F**.

skeleton of **BN[8]H**, the lengths of the B–N bond and B–C bonds increased after coordination with fluoride, from 1.417, 1.544, and 1.561 Å to 1.531, 1.642, and 1.623 Å (Fig. S19), respectively. The dihedral angle (ring A' and ring B') and the distance of C27···C35 increases to 60.77° and 3.37 Å (Fig. S20 in Supporting information), respectively. In the packing diagram, tetrabutylammonium ions are uniformly dispersed in 2D supramolecular sheet framework of **BN[8]H-F** and broken the intermolecular B···B interactions. The homochiral isomers stack along the *a*-axis through multiple intermolecular interactions (F···H, F···C, S···H, C···H, and H···H) and the heterochiral molecules are stacked along the *c*-axis through intermolecular S···S interactions (Fig. S21 in Supporting information). The details of crystal structures are shown in Fig. S23 (Supporting information), and the crystal parameters are listed in Table S8 (Supporting information).

The chiral resolutions of **BN[8]H** was successfully resolved by chiral HPLC (Fig. S15 in Supporting information). The optical rotations of (+)-**BN[8]H**, $[\alpha]_D^{25} = +1864°$ ($c = 0.95$ mg/mL in DCM) and (-)-**BN[8]H**, $[\alpha]_D^{25} = -1875°$ ($c = 0.96$ mg/mL in DCM) were observed, respectively. The CD and CPL spectra of the enantiomers of **BN[8]H** are depicted in Fig. 3. CD were measured in DCM at room temperature. Enantiomerically pure **BN[8]H** exhibit obvious Cotton effects in the range from 250 nm to 450 nm, with the maximum positive Cotton effects at 271 nm, respectively, with perfect mirror-image profiles in the CD spectra (Fig. 3a). The CPL spectra of (+)-**BN[8]H** and (-)-**BN[8]H** showed perfect mirror image (Fig. 3b). The luminescence dissymmetry factors g_{lum} were 6.2×10^{-3} and -6.5×10^{-3}. Surprisingly, under TABF treatment, the ECD signs significant inverted and a new strong band emerged around 374 nm, corresponding to the peak of UV–vis spectra. The CPL spectrum of **BN[8]H-F** showed an inversion with a slight decrease in signal intensity and g_{lum} (-5.1×10^{-4} and 5.3×10^{-4}) (Fig. 4d, Figs. S16 and S17 in Supporting information). These experimental results prove the formation of **BN[8]H-F**. Although this g_{lum} value is lower than those observed in some supramolecular systems [54,55], liquid crystal systems [25–27] and other π-extended or multiple helicenes [47,48], but it remains at an intermediate level among small-molecule helicene systems. Importantly, we present a strategy for achieving chiral inversion using simple ionic stimuli, offering a novel design approach for chiral inversion and stimuli-responsive materials. Upon adding $BF_3{\cdot}Et_2O$ to the **BN[8]H-F** solution, the CD and CPL signals reverted to the initial peak position of **BN[8]H** (Figs. S16 and S17 in Supporting information), confirming the dissociation of the fluoride-boron coordinate bond. The dissymmetry factor (g_{lum}) for the CPL can be described using the transition electronic dipole moment (μ), the transition magnetic dipole moment (m), and the angle between the μ and m vectors (θ) according to $g_{lum} = 4|\mu|\cdot|m|\cos\theta/(|\mu|^2 + |m|^2)$. The θ has a direct impact on the CPL signal. Therefore, for a deeper understanding of the mechanism of fluoride-induced ECD and CPL inversion of **BN[8]H**. To ensure the accuracy of theoretical calculations, we evaluated the effects of multiple functionals on the glum of **BN[8]H** (Tables S4-S6 in Supporting information). The final results indicate that B3LYP/6–31G(d,p) is a more suitable functional for **BN[8]H**. Time-dependent density functional theory (TD-DFT) (B3LYP(BJ)/6–31G(d,P)-PCM) calculations were conducted, Fig. 4 presents the calculated μ and m of **BN[8]H** and **BN[8]H-F**. The angle between the two dipolemoments is 72.9° for **BN[8]H** and 101.3° for **BN[8]H-F**, suggesting their opposite CPL signals, the calculated $g_{lum,cal}$ values were $\pm 5.5 \times 10^{-4}$, which agrees with the experimental results.

To evaluate the conformational stability, the racemization process of **BN[8]H** and **BN[8]H-F** was estimated by DFT calculation at the B3LYP/6–31G(d,p) level. As shown in Fig. 3c, the energy barrier required for the transformation from (*M*)-**BN[8]H** to (*P*)-**BN[8]H** was 39.2 kcal/mol. After treatment with TABF, the energy barrier was increased to 47.5 kcal/mol. These experimental results suggest

that **BN[8]H** and **BN[8]H-F** maintain stable chirality that is resistant to flipping.

In summary, we have efficiently synthesized a new boron–nitrogen infused heterohelicene, **BN[8]H** *via* Suzuki coupling and intramolecular electrophilic arene borylation reactions. The helical structures of **BN[8]H** and **BN[8]H-F** were con-firmed by X-ray single crystal analysis. Enantiomers **BN[8]H** showed a fluoride-induced sign inversion of both ECD and CPL. TD-DFT calculations revealed that the fluoride ions significant influence the transition dipole moments and $\theta_{u,m}$, resulting in CPL reversal. This study establishes a new strategy to efficiently and conveniently adjust the handedness and intensity of CPL of helicenes based on B,N-embedded molecular system. We believe that this finding can help providing a deep insight in regulating the chiroptical behaviors of helicenes and highlighting the potential for integrated chiral electronics and photonics.

Declaration of competing interest

The authors declare that they have no known competing financial interests or personal relationships that could have appeared to influence the work reported in this paper.

CRediT authorship contribution statement

Shuai Qiu: Writing – original draft, Investigation, Formal analysis, Data curation. **Jia Tang:** Formal analysis. **Wan Xu:** Formal analysis. **Zhiying Ma:** Data curation. **Chao Zhang:** Formal analysis. **Sheng Zhang:** Funding acquisition, Formal analysis, Data curation. **Chunli Li:** Software, Investigation. **Wei Tian:** Writing – review & editing, Supervision. **Hua Wang:** Writing – review & editing, Methodology, Funding acquisition.

Acknowledgments

This work was financially supported by the National Natural Science Foundation of China (Nos. 22471061, U2004213, 22475063), Natural Science Foundation of Henan (Nos. 242300421607, 242300421611, 252300420754), China Postdoctoral Science Foundation (No. 2023M730951) and Open Foundation project of Henan University (No. DCSHENU2420).

Supplementary materials

Supplementary material associated with this article can be found, in the online version, at doi:10.1016/j.cclet.2025.111778.

References

[1] X. Zou, N. Gan, Y. Gao, et al., Angew. Chem. Int. Ed. 64 (2025) e202417906.
[2] J. Liu, X. Zhou, X. Tang, et al., Adv. Funct. Mater. 35 (2025) 2414086.
[3] Y.J. Long, X.N. Han, Y. Han, et al., Chin. Chem. Lett. 36 (2025) 110600.
[4] L.E. MacKenzie, R. Pal, Nat. Chem. Rev. 5 (2021) 109–124.
[5] M. Zhang, Q. Guo, Z. Li, et al., Sci. Adv. 9 (2023) eadi9944.
[6] L. Wan, R. Zhang, E. Cho, et al., Nat. Photonics 17 (2023) 649–655.
[7] C. Wang, T. Jiang, X. Ma, Chin. Chem. Lett. 31 (2020) 2921–2924.
[8] S. Huo, P. Duan, T. Jiao, Q. Peng, M. Liu, Angew. Chem. Int. Ed. 129 (2017) 12342–12346.
[9] D. Zhang, C.Y. Yu, L. Zheng, et al., Chin. Chem. Lett. 31 (2020) 673–676.
[10] K. Takaishi, K. Iwachido, T. Ema, J. Am. Chem. Soc. 142 (2020) 1774–1779.
[11] X. Song, X. Zhu, S. Qiu, et al., Angew. Chem. Int. Ed. 61 (2022) 8574–8583.
[12] J. Bao, R. Lan, C. Shen, et al., Adv. Optical Mater. 10 (2022) 2101910.
[13] F. Wang, W. Ji, P. Yang, et al., ACS Nano 13 (2019) 7281–7290.
[14] X. Wang, Q. Song, Z. He, et al., Chin. Chem. Lett. 36 (2025) 110047.
[15] K. Yao, Z. Liu, H. Li, et al., Sci. China Chem. 65 (2022) 1945–1952.
[16] A.H.G. David, R. Casares, J.M. Cuerva, et al., J. Am. Chem. Soc. 141 (2019) 18064–18074.
[17] M. Xu, Z. Xu, M.A. Soto, et al., Adv. Mater. 35 (2023) 2301060.
[18] S. Ghorai, S. Show, A. Das, Angew. Chem. Int. Ed. 64 (2025) e202500879.
[19] M.Y. Zhang, X. Liang, D.N. Ni, et al., Org. Lett. 23 (2021) 2–7.
[20] K. Yao, Z. Wang, P. Wang, et al., Angew. Chem. Int. Ed. 64 (2025) e202420290.
[21] W. Li, S. Yin, Z. Song, et al., Inorg. Chem. Front. 12 (2025) 1176–1186.
[22] Y. Zhang, J. Wang, H. Chen, et al., Chin. Chem. Lett. 33 (2022) 2473–2476.
[23] K. Fu, G. Liu, ACS Nano 18 (2024) 2279–2289.
[24] R. Ren, Y. Pan, H.X. Wang, et al., Chin. Chem. Lett. 36 (2025) 111060.
[25] J. Liu, Z.P. Song, L.Y. Sun, et al., Responsive Mater. 1 (2023) e20230005.
[26] S. Li, J. Wang, M. Tian, et al., Angew. Chem. Int. Ed. 63 (2024) e202405615.
[27] W. Kang, Y. Tang, X. Meng, Angew. Chem. Int. Ed. 62 (2023) e202311486.
[28] Y. Shen, C.F. Chen, Chem. Rev. 112 (2012) 1463–1535.
[29] W.L. Zhao, M. Li, H.Y. Lu, et al., Chem. Commun. 55 (2019) 13793–13803.
[30] J.F. Xing, K. Li, W. Xiang, et al., Chin. Chem. Lett. (2025) 110982.
[31] T. Mori, Chem. Rev. 121 (2021) 2373–2412.
[32] W.B. Lin, M. Li, L. Fang, et al., Chin. Chem. Lett. 29 (2018) 40–46.
[33] W.W. Yang, J.J. Shen, Chem. Eur. J. 28 (2022) e202202069.
[34] I. Shioukhi, H. Batchu, G. Schwartz, et al., Angew. Chem. Int. Ed. 63 (2024) e202319318.
[35] Y. Gisbert, M. Ovalle, C.N. Stindt, et al., Angew. Chem. Int. Ed. 64 (2025) e202416097.
[36] W.B. Lin, D.Q. He, H.Y. Lu, et al., Chem. Commun. 56 (2020) 1863–1866.
[37] S. Miwa, D. Mizutani, K. Kawano, et al., Chem. Eur. J. 31 (2025) e202500335.
[38] H.W. Li, M. Li, Z.H. Zhao, et al., Org. Lett. 23 (2021) 4759–4763.
[39] E. Yen-Pon, F. Buttard, L. Frédéric, et al., JACS Au 1 (2021) 807–818.
[40] D. Tan, J. Dong, T. Ma, et al., Angew. Chem. Int. Ed. 62 (2023) e202304711.
[41] D. Volland, J. Niedens, P.T. Geppert, et al., Angew. Chem. Int. Ed. 62 (2023) e202304291.
[42] Y. Appiarius, S. Míguez-Lago, P. Puylaert, et al., Chem. Sci. 15 (2024) 466–476.
[43] A. Nowak-Król, P.T. Geppert, K.R. Naveen, Chem. Sci. 15 (2024) 7408–7440.
[44] C. Maeda, K. Nagahata, T. Shirakawa, et al., Angew. Chem. Int. Ed. 59 (2020) 7813–7817.
[45] J. Full, S.P. Panchal, J. Götz, Angew. Chem. Int. Ed. 60 (2021) 4350–4357.
[46] F. Zhang, V. Brancaccio, F. Saal, et al., J. Am. Chem. Soc. 146 (2024) 29782–29791.
[47] Y. Yu, C. Wang, F.F. Hung, et al., J. Am. Chem. Soc. 146 (2024) 22600–22611.
[48] Y. Yu, C. Wang, F.F. Hung, et al., Angew. Chem. Int. Ed. 64 (2025) e202501645.
[49] Z. Ye, H. Wu, Y. Xu, et al., Adv. Mater. 36 (2024) 2308314.
[50] L. Dang, W. Xu, S. Qiu, et al., Org. Lett. 26 (2024) 10141–10145.
[51] W. Xu, J. Wei, K. Tang, et al., Org. Chem. Front. 9 (2022) 5578–5585.
[52] H.R. Bhat, P.S.S. Gupta, S. Biswal, et al., ACS Omega 4 (2019) 4505–4518.
[53] V.M. Hertz, N. Ando, M. Hirai, et al., Organometallics 36 (2017) 2512–2519.
[54] W. Yuan, L. Chen, C. Yuan, et al., Nat. Commun. 14 (2023) 8022.
[55] K. Fu, D.H. Qu, G. Liu, J. Am. Chem. Soc. 146 (2024) 33832–33844.